IMPROVING THE IMAGING RESOLUTION OF 3D PSTM IN VTI MEDIA USING OPTIMAL SUMMATION WITHIN THE FRESNEL ZONE

HAO ZHANG[1], JIANGJIE ZHANG[1], ZHENGWEI LI[1], JIANFENG ZHANG[1] and JIANG XIAO[2]

[1] *Key Laboratory of Petroleum Resources Research, Institute of Geology and Geophysics, Chinese Academy of Sciences, Beijing 100029, P.R. China. zhanghao@mail.iggcas.ac.cn*
[2] *Geophysical Research Institute, BGP Inc., China National Petroleum Corporation, Korla, Xinjiang 841001, P.R. China.*

(Received September 2, 2016; revised version accepted May 11, 2017)

ABSTRACT

Zhang, H., Zhang, J., Li, Z., Zhang, J. and Xiao, J., 2017. Improving the imaging resolution of 3D PSTM in VTI media using optimal summation within the Fresnel zone. *Journal of Seismic Exploration*, 26: 311-330.

We improve the amplitude-preserved PSTM in 3D VTI media by introducing a stationary-phase implementation in dip-angle domain so as to achieve optimal summation within Fresnel zone. The previous proposed amplitude-preserved PSTM scheme in 3D VTI media has been proven effective to produce fine image and gathers for hydrocarbon and fluid detection. However, due to the application of a relatively simple migration aperture, this migration scheme may suffer from migration noise and degrade the resolution gained. The proposed implementation in this paper can improve the 3D VTI PSTM by smearing each time sample only along the Fresnel zone rather than along the whole migration aperture, thus suppressing the noises on 3D VTI PSTM result. The Fresnel zone range is defined by picking up dip angles on dip-angle gathers generated from VTI PSTM scheme thus noises outside the Fresnel zones are suppressed in the migration process. The proposed stationary-phase VTI PSTM could effectively solve the problem of low signal-to-noise ratios in migrated images, especially in the presence of steeply dipping structures. We apply the so-called stationary-phase amplitude-preserved VTI PSTM to a field data. An improved imaging result is obtained.

KEY WORDS: stationary-phase, pre-stack time migration, Fresnel zone, noise suppression.

0963-0651/17/$5.00

INTRODUCTION

An amplitude-preserved PSTM scheme in 3D vertical transverse isotropic (VTI) media was developed following the conventional PSTM previously (Zhang and Zhang, 2012). This Kirchhoff-like migration scheme has many good features for large scale production purpose in seismic industry, such as simplicity, relatively low computational cost, tolerance of using irregular observation geometries as well as allowing appreciation and updating both migration velocity and anisotropic parameter. A practical problem of this kind of migration scheme is the presence of migration noise and artifact, which can be the outcome of a redundant global migration aperture and aliasing of the migration operator. Regarding the influence of imaging quality from migration aperture, Sun (1998, 1999) analyzes the effect of restricting the domain of migration aperture to imaging results in two-dimensional data and points out that the data outside the Fresnel zone has not a substantial contribution to imaging, and may even deteriorates the imaging quality by introducing migration artifacts. Besides, due to the realization of the migration algorithm, in a migration operation, we tend to select a global migration aperture. However, the dip-angles of structures are spatially varying, particular in the presence of steeply dipping structures. When the selected aperture is appropriate to a certain imaging point, it may be larger or smaller to other imaging points.

There are many approaches intended to reduce the imaging noise by limitation of the migration aperture. Schleicher et al. (1997) define a minimum migration aperture based on the so-called projected Fresnel zone. Tillmanns and Gebrande (1999) use time domain event slope information to build a heuristic weight function which limited the migration aperture. Sun and Schuster (2001) use the same information to transform the diffraction stack integral under the stationary phase approximation. This formulation allows smearing energy along a small zone centered at the specular reflection point. Buske et al. (2009) propose an optimal anti-aliasing filter using pre-stack slope information as well. The common challenge for these previous works is the estimation of Fresnel zone by the slope picking procedure in pre-stack data domain to constrain the migration operator.

Accurate estimation of the Fresnel zone can be influenced by migration velocity, data frequencies and reflector dips. Even the reflector dips are extracted from migration implementation (Chen, 2004) or stacked migration section (Marfurt, 2006), obtaining accurate Fresnel zones is yet difficult. Klokov and Fomel (2012a) estimated the Fresnel zones by jointly using the migrated dip-angle gathers and migrated stacked section. Yu et al. (2013) directly remove non-flat energy in the migrated dip-angle gathers to achieve stacking within the Fresnel zones. The estimation of the Fresnel zones becomes more challenging in 3D cases (Okoye and Uren, 1992).

In this work, to achieve an optimal migration result with less migration noise, we implement the amplitude-preserved 3D VTI PSTM scheme using optimal summation aperture based on stationary-phase theory. This implementation smears each time sample only along the Fresnel zone rather than along the whole migration aperture. The algorithm in this paper operates in dip-angle domain after migration and makes use of auto-picking technique of dip-angle parameters which defines the range of the Fresnel zones for summation.

This paper is arranged as follows: First, we introduce the method of yielding the dip-angle gathers in time domain from 3D VTI PSTM scheme. We then present the estimation of the 2D Fresnel zones using auto-picking technique. Finally, we apply the resulting stationary-phase 3D amplitude-preserved VTI PSTM to a real dataset. As the 3D amplitude-preserved VTI PSTM is proposed previously, we will review its theory and basic theoretical aspects as an Appendix.

DIP-ANGLE GATHERS GENERATION USING 3D VTI PSTM

Starting from the analytical derivation of 3D VTI PSTM (see Appendix A), the stationary point (p_x^0,p_y^0) obtained at imaging location (x,y,T) that reads

$$p_x^0 = (x - x_g)/V_{rms}[V_{rms}^2T^2 + (x - x_g)^2 + (y - y_g)^2]^{1/2} , \tag{1a}$$

$$p_y^0 = (y - y_g)/V_{rms}[V_{rms}^2T^2 + (x - x_g)^2 + (y - y_g)^2]^{1/2} . \tag{1b}$$

Fig. 1 gives the illustration of dip-angle gather generation from the seismic data. Using eq. (1) and ignoring the difference between the interval and RMS velocities (Zhang et al., 2016), we derive the direction cosines of scattered-ray at imaging point (x,y,T) approximately as

$$l_g = vp_x^g = (x - x_g)/[(x - x_g)^2 + (y - y_g)^2 + V_{rms}^2T^2]^{1/2} , \tag{2a}$$

$$m_g = vp_y^g = (y - y_g)/[(x - x_g)^2 + (y - y_g)^2 + V_{rms}^2T^2]^{1/2} , \tag{2b}$$

$$n_g = [1 - l_g^2 - m_g^2]^{1/2} , \tag{2c}$$

and direction cosines of incident-ray at imaging point (x,y,T) as

$$l_s = vp_x^s = (x - x_s)/[(x - x_s)^2 + (y - y_s)^2 + V_{rms}^2T^2]^{1/2} , \tag{3a}$$

$$m_s = vp_y^s = (y - y_s)/[(x - x_s)^2 + (y - y_s)^2 + V_{rms}^2T^2]^{1/2} , \tag{3b}$$

$$n_s = [1 - l_s^2 - m_s^2]^{1/2} , \tag{3c}$$

where T is the vertical one-way traveltime, V_{rms} is the root-mean-square (RMS) velocity at the imaging point, respectively. (x_g,y_g) and (x_s,y_s) are the lateral coordinates of the receiver and shot, and subscripts or superscripts g and s denote scattered and incident rays, respectively.

From the perspective of imaging, the scattered-ray represents a reflection for the incident-ray to hit the reflector at the imaging point. The normal vector to the reflector at the imaging point can be expressed as (l_0,m_0,n_0) due to that the scattered-ray represents a reflection for the incident-ray to hit the reflector

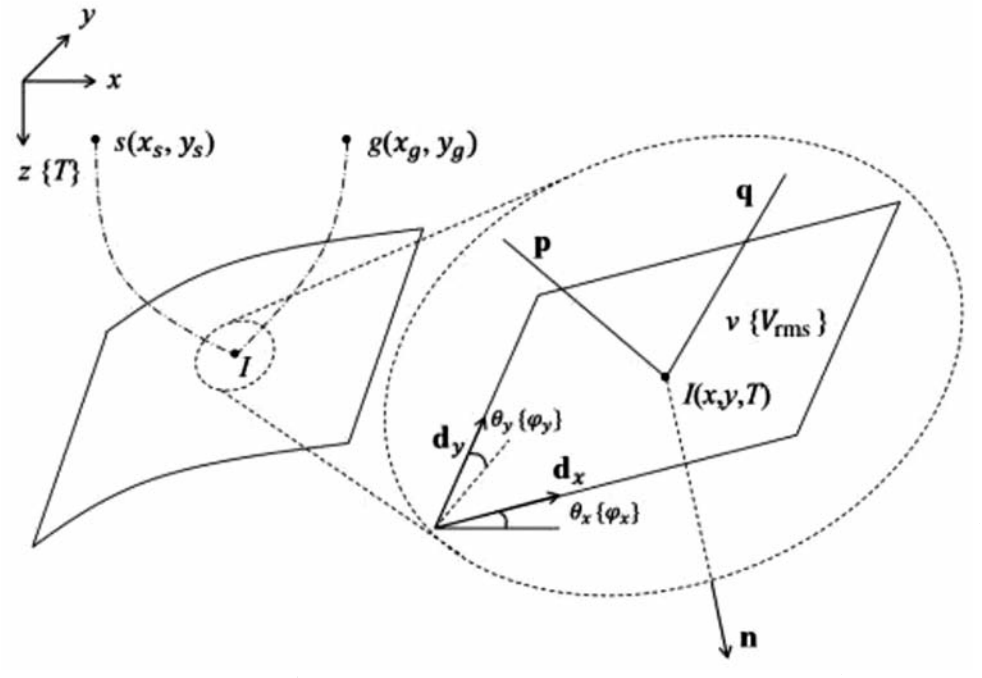

Fig. 1. Illustration of the generation of the dip-angle gather. Point I denotes the imaging point. Points s and g denote shot and receiver, respectively. The right side is the enlarged detail in the neighborhood of imaging point I. The local reflector at imaging point I can be assumed as a tilted plane. Vectors **p** and **q** denote the scattered and incident-rays at imaging point I, respectively. Vector **n** is the normal to the local reflector. Vectors $\mathbf{d}_x$ and $\mathbf{d}_y$ denote the intersections of the local reflector with the xz- and yz-planes of the coordinate system, respectively. Angles θ_x and θ_y are the apparent dips of the local reflector in the xz- and yz-planes. The interval velocity at imaging point I is defined as v. Braces indicate the variables, such as φ_x, φ_y, and V_{rms}, expressed in the vertical traveltime coordinate system.

at the imaging point. θ_x and θ_y denote the dip-angles of the reflector in inline and crossline direction, respectively. Then we have the vector $(\cos\theta_x,0,\sin\theta_x)$ and $(0,\cos\theta_y,\sin\theta_y)$ to be orthogonal with the normal to the reflector, respectively. That yields

$$\tan\theta_x = -l_0/n_0 \quad , \tag{4a}$$

$$\tan\theta_y = -m_0/n_0 \quad . \tag{4b}$$

The migrated dip-angle gathers are generated and the Fresnel zones explicitly exhibit in the resulting gathers. Because the approximated dip-angles do not change the characters of the dip-angle gathers, we replace the true dip-angles θ_x and θ_y with approximated ones. The approximated dip-angles are termed as the traveltime related dip-angles here. In practice, the traveltime related dip-angles represent the reflector dips extracted from the imaging volume in time, as explained in eq. (B-4) (see Appendix B). From eq. (4), we obtain the traveltime related dip-angles of the reflector, φ_x and φ_y in both inline and crossline direction as

$$\tan\varphi_x = [(x_s - x)\tau_g + (x_g - x)\tau_s]/(\tau_s + \tau_g)V_{rms}T \quad , \tag{5a}$$

$$\tan\varphi_y = [(y_s - y)\tau_g + (y_g - y)\tau_s]/(\tau_s + \tau_g)V_{rms}T \quad , \tag{5b}$$

where τ_s and τ_g are the traveltimes from the shot (x_s,y_s) and receiver (x_g,y_g) to the imaging point (x,y,T), respectively. Integrating the solutions of eq. (5) into the VTI PSTM scheme, we can obtain a couple of dip-angle gathers at each lateral position by summation of the corresponding migrated result that share the same φ_x or φ_y at each imaging point (x,y,T) regardless of offsets, respectively. $f_m(t)$ denotes the time series of the m-th trace of migration input data. Following the discussion in Appendix A, we have a couple of dip-angle gathers over 3D imaging volume as

$$G_x(x,y,T_0,\varphi_x) = \sum_{m=1}^{n} (\tau_s^2/\tau_g^2) f'_m(\tau_s+\tau_g;x_s,y_s,x_g,y_g) \quad , \tag{6a}$$

$$G_y(x,y,T_0,\varphi_y) = \sum_{m=1}^{n} (\tau_s^2/\tau_g^2) f'_m(\tau_s+\tau_g;x_s,y_s,x_g,y_g) \quad , \tag{6a}$$

where $T_0 = 2T$ is the two-way vertical traveltime, n is the number of the seismic traces, $f'_m(t)$ is the first-order time derivative of $f_m(t)$, and τ_s and τ_g are the traveltimes from the shot (x_s,y_s) and receiver (x_g,y_g) to the imaging point (x,y,T), respectively.

At each lateral position (x,y), $G_x(T_0,\varphi_x)$ and $G_y(T_0,\varphi_y)$ represent a couple of 1D migrated gather in terms of traveltime related inline or crossline dip-angle, respectively. Similar to the dip-angle gather obtained using 2D depth migration (Landa et al., 2008; Klokov and Fomel, 2012a, 2012b; Giboli et al., 2013), the reflections resulting from planar reflectors will exhibit concave shapes in the migrated gathers, and the Fresnel zones (related to the reflection events) just cover the flat part around the apexes of concave shapes independent of velocities and reflector dips. Hence, the dip-angle gathers can be regarded as a good candidate and simple domain for Fresnel zone estimation.

Following eqs. (6a) and (6b), we can further derive the 2D dip-angle gathers over 3D volume by summing the migrated result with the same traveltime-related dip angle (φ_x,φ_y) at each imaging point (x,y,T) regardless of offset as

$$G_y(x,y,T_0,\varphi_y) = \sum_{m=1}^{n} (\tau_s^2/\tau_g^2) f'_m(\tau_s+\tau_g;x_s,y_s,x_g,y_g) \quad . \tag{7}$$

ESTIMATION OF FRESNEL ZONES IN THE DIP-ANGLE DOMAIN

After generating dip-angle gathers from migration, we note that migrated reflection events have concave shapes, and the apex of the curve corresponds to the dip-angle, due to the stacking of the migrated dip-angle gathers along the direction of the dip-angle. According to stacking, in the image domain, the apex is the stationary point and the flat parts around the apex are the Fresnel zones. In dip-angle domain, Fresnel zone is directly exhibited thus it can be determined from the migrated dip-angle gathers, which avoids direct calculation of the Fresnel zone. The details of Fresnel zone in dip-angle domain are demonstrated in Appendix B. Fig. 2 gives an example that demonstrates the Fresnel zone range in the dip-angle domain, the ellipse (black line) Fresnel zones are put on the local time slice of the dip-angle gather around the event apex. The 2D Fresnel zones are obtained using the proposed scheme based on the dip-angle gathers generated.

The Fresnel zone actually corresponds to the approximately horizontal part of the hyperbolic reflector. Defining $a_{i,j}$ as the amplitude of the gather that has the time sample index i and dip-angle sample index j, with $b_{ij} = \min(a_{i-1,j},a_{i,j},a_{i+1,j})$, we can use the following indicator I to judge whether (i,j) is the stationary point, which further determines whether the event passing through the sample point is horizontal. The indicator formula related to the event flatness is expressed as

$$I = \Big| \sum_{k=j-m_1}^{j+m_2} b_{ik} \Big| \Big/ \sum_{k=j-m_1}^{j+m_2} |b_{ik}| \quad , \tag{8}$$

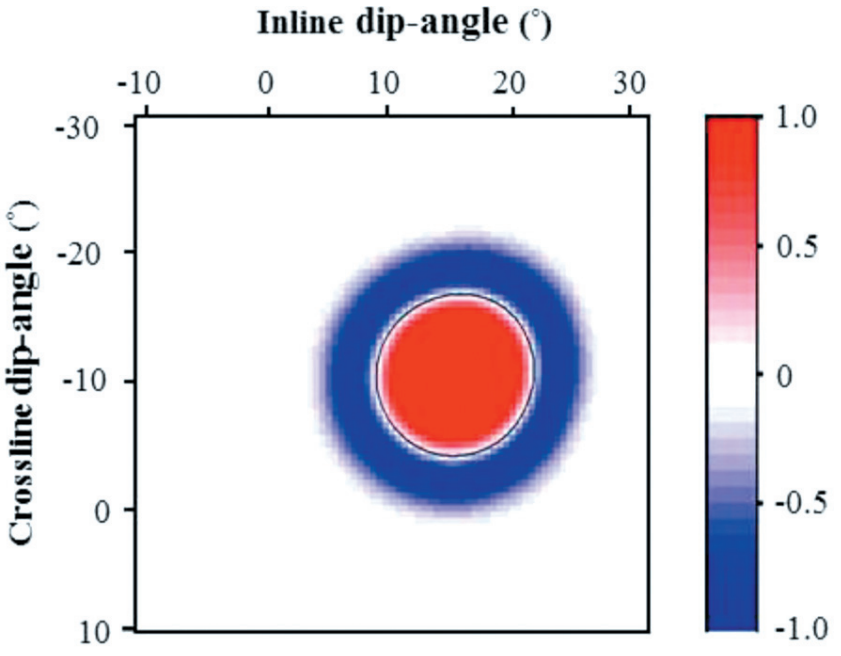

Fig. 2. An example of 2D Fresnel zones in dip-angle domain. The ellipse is in black circle on the local time slice around the 2D event apex. The bar shows the magnitude of the normalized amplitudes on the time slice.

where m_1 and m_2 denote the lower and upper limits of the Fresnel zone dip-angles, respectively. I equals to 1 when the event is absolutely horizontal. The choice of m_1 and m_2 is very important, because if they are too close, there will be a large number of sample points that satisfy the criterion and the true stationary point will not be outstanding.

In this paper, we estimate the Fresnel zone in the dip-angle domain using stacked zero offset data to determine parameters m_1 and m_2. The idea is that if a ray is shot from the imaging point, which is the edge of the reflection interface used to define the stationary point, then the traveltime to the receiver point and from the receiver point to the point one-quarter cycle above the stationary point will be identical in terms of the time difference. Using the conditions of the two known dip-angles and the traveltime at the stationary point, we can obtain the edge curve of the Fresnel zone on the reflection interface. On this interface, the curve is regarded as a circle with radius

$$d = V_{rms}\sqrt{\{T/(2f_0)\}} \quad , \tag{9}$$

where f_0 is the main frequency and T is the time depth of the stationary point.

We can obtain the edge curve by calculating the two aforementioned dip angles. Because these two migrated dip-angle gathers are the result of the superposition in terms of the two dip-angles, information about the edge curve is contained within them. For the gathers selected along the inline direction, the lower and upper limits of the dip-angle value are the minimum and maximum of the edge curve that corresponds to dip-angle along the inline direction. For the crossline direction, the same condition applies. The two migrated dip-angle gathers, m_1 and m_2, read as

$$\begin{aligned} m_1 &= (1/\Delta\varphi)\{\varphi_j - \arctan[1/[1-1/(2T_if_0)] \\ &\quad \times [\tan\varphi_j - \sqrt{\{(1/T_if_0)[1-1/(24_if_0)](1+\tan^2\varphi)\}}]\} \ , \\ m_2 &= (1/\Delta\varphi)\{\arctan[1/[1-1/(2T_if_0)] \\ &\quad \times [\tan\varphi_j + \sqrt{\{(1/T_if_0)[1-1/(24_if_0)](1+\tan^2\varphi)\}}] - \varphi_j\} \ , \end{aligned} \tag{10}$$

where T_i is the time depth, $\Delta\varphi$ is the sample interval of the dip-angle, and φ_j is the dip-angle in the inline or crossline direction.

Isolated large amplitude may lead to deviant large results when calculation eq. (10), therefore we need to exclude samples that are obviously not the stationary point. We calculate the average value using the formula

$$F = \sum_{k=j-m_1}^{j+m_2} |b_{ik}|/(m_2 - m_1 + 1) \ . \tag{11}$$

We only utilize eq. (10) when the average value exceeds the defined threshold.

In determination of the upper and lower limit for the Fresnel zone using eqs. (8) to (11), for each stationary point, we calculate $m_1 = m_1 + 1$ and $m_2 = m_2 + 1$ to determine coefficients I and F, respectively. When the conditions are not satisfied, we record the corresponding m_1 and m_2 and take the Fresnel zone width as $m_2 - m_1 + 1$. If multiple stationary points exist, we only retain the point with maximum width. If the value is close to the maximum width, we only retain that closest to the zero dip-angle corresponding to m_1 and m_2. For all of the stationary points at every time depth, we select the minimum value of m_1 and the corresponding dip-angle φ_1 with time depth T_1 and the maximum value of m_2 and the corresponding dip-angle φ_2 with time depth T_2. Then, the dip-angles $\varphi_1 - m_1 \cdot \Delta\varphi$ at T_1 and $\varphi_2 + m_2 \cdot \Delta\varphi$ at T_2 jointly constitute the upper and lower boundary of the Fresnel zone.

Then, the obtained upper and lower limits of the Fresnel zone should be interpolated along the time depth direction, giving the so-called edge curve of the Fresnel zone in the CDP location. It is very obvious to visually review the Fresnel zone, project it to the migrated dip-angle gathers. By interpolating all of the edge curves, we can obtain all of the Fresnel zone parameters in the dip-angle domain. We finally sum the migration result using the 2D Fresnel zone obtained, the VTI PSTM with optimal summation could be achieved.

FIELD DATA EXAMPLE

To demonstrate the effectiveness of our method, we test our methodology on a real 3D land dataset acquired from Songliao Basin, northeastern China. The data set is acquired by swath shooting. Each swath contains 12 receiver cables spaced at 200 m. The shot interval is 100 m along each shot-line. A typical shot record has 12×160 traces with a receiver group interval of 50 m. The data are sampled at 2 ms with a length of 4 s. Offsets of the data set vary around 50 to 4620 m. We migrate the data set to obtain an imaging volume that consists of 281 (Lines) $\times$ 651 (CDPs) with a line spacing of 25 m and CDP spacing of 25 m.

Fig. 3 displays the work flow chart of our method, and the key processing steps are the generation of the migrated dip-angle gathers and estimation the range of the Fresnel zones, which determines the result quality of the new VTI PSTM scheme. Fig. 4 shows a typical set of conditioned shot gathers for migration. Then we use the work flow described in (Zhang and Zhang, 2012) to derive the migration velocity field and the anisotropic parameter sequentially. Fig. 5 shows the migration velocity of line 181 used for migration processing, the lateral velocity variation is not very intense thus the PSTM approach is appropriate to process this data. Fig. 6 shows the corresponding effective anisotropic parameter estimated using gather flatness scanning. Using the migration velocity and the anisotropic parameter, we begin to generate the dip-angle gathers following the flow illustrated in Fig. 3.

Fig. 7 shows a typical couple of dip-angle gathers in inline and crossline direction overlaid with the Fresnel range using our method. The two white lines on each figure denote the lower and upper limits of the Fresnel zones obtained by the proposed scheme. The estimated Fresnel zones accurately cover the apexes and flat parts of concave shapes. With the Fresnel zone defined using the auto-picking technique, we can achieve the optimal summation within the estimated Fresnel zone and generate better migration result. Fig. 8 shows the migration result of inline 181 and crossline 341 using the proposed VTI PSTM with optimal summation. The main events and faults are well imaged.

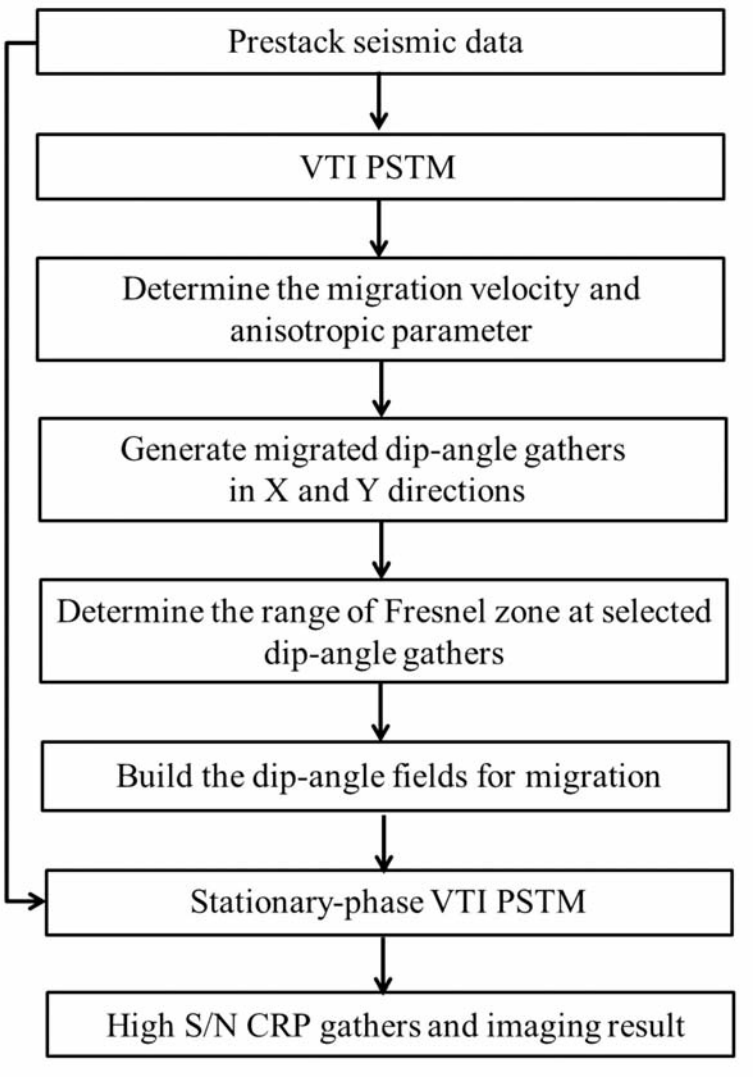

Fig. 3. Work flow chart of stationary-phase VTI PSTM. The key steps are the generation of migrated dip-angle gathers and Fresnel zone estimation.

To assess the effects of the stationary-phase VTI PSTM, we apply the conventional VTI PSTM as described in (Zhang and Zhang, 2012) without optimal summation to the same data set as a reference and make a comparison. Fig. 9 compares the migrated stacked sections on inline 181. Obvious signal-to-noise ratio improvements can be seen. In addition, we extract the time slice at 2.3 s (Fig. 10) from the migration volume on which we can identify the faulting system and channels more easily. Better resolution on Fig. 10b can be seen which is produced by the new method.

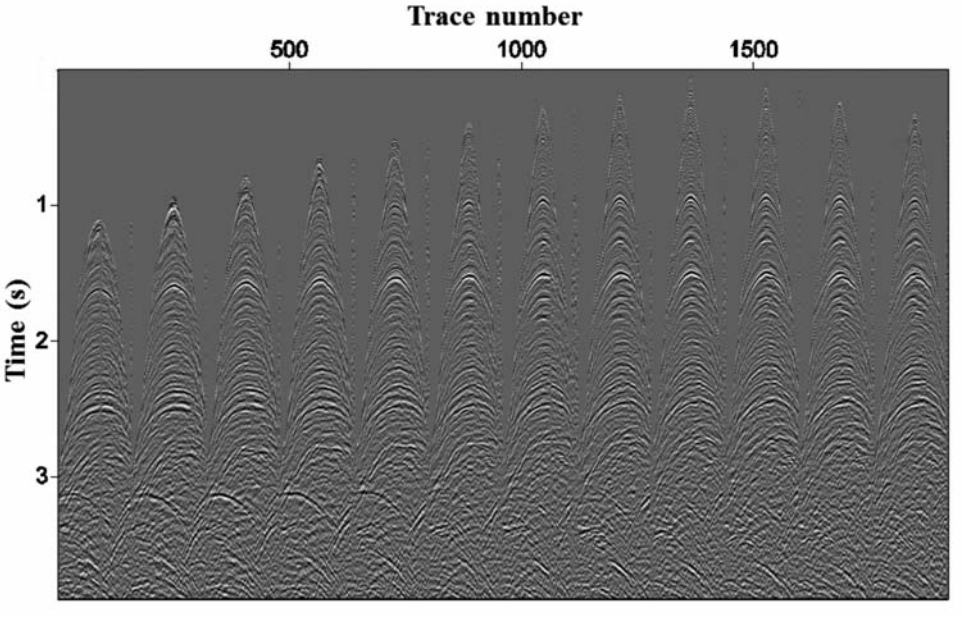

Fig. 4. Typical shot gathers of the 3D field data. Each shot record contains 12 receiver lines.

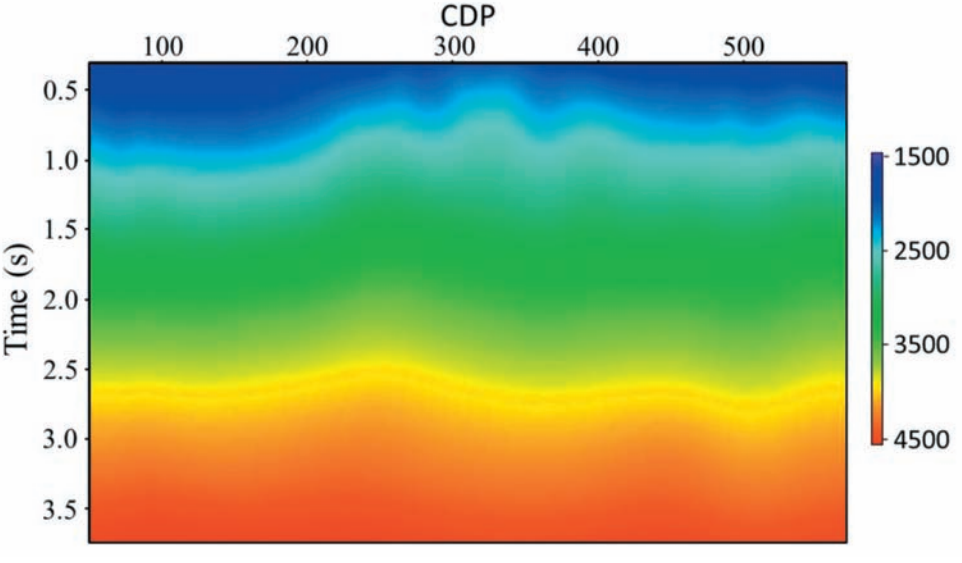

Fig. 5. Migration V_{rms} velocity field used for 3D VTI PSTM (Line 181). Note that the time axe is related to the vertical two way traveltime.

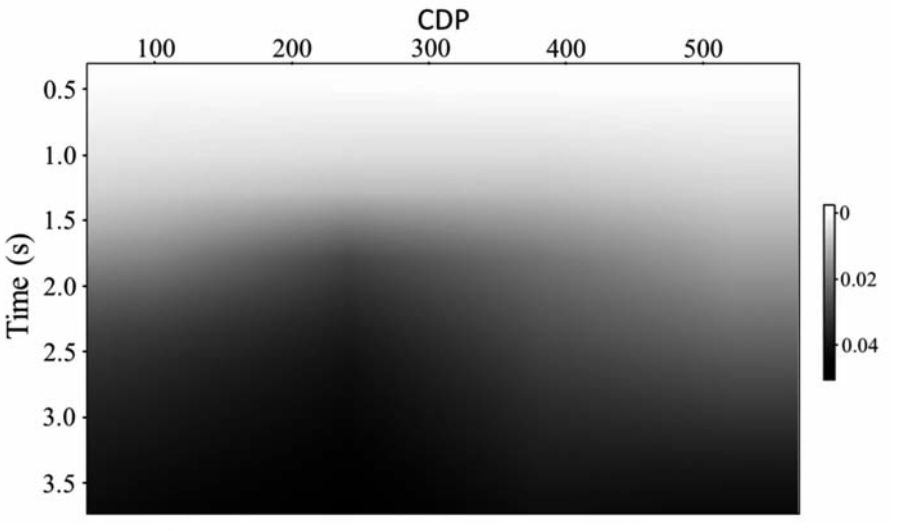

Fig. 6. Estimated anisotropic parameter field used for VTI migration (Line 181).

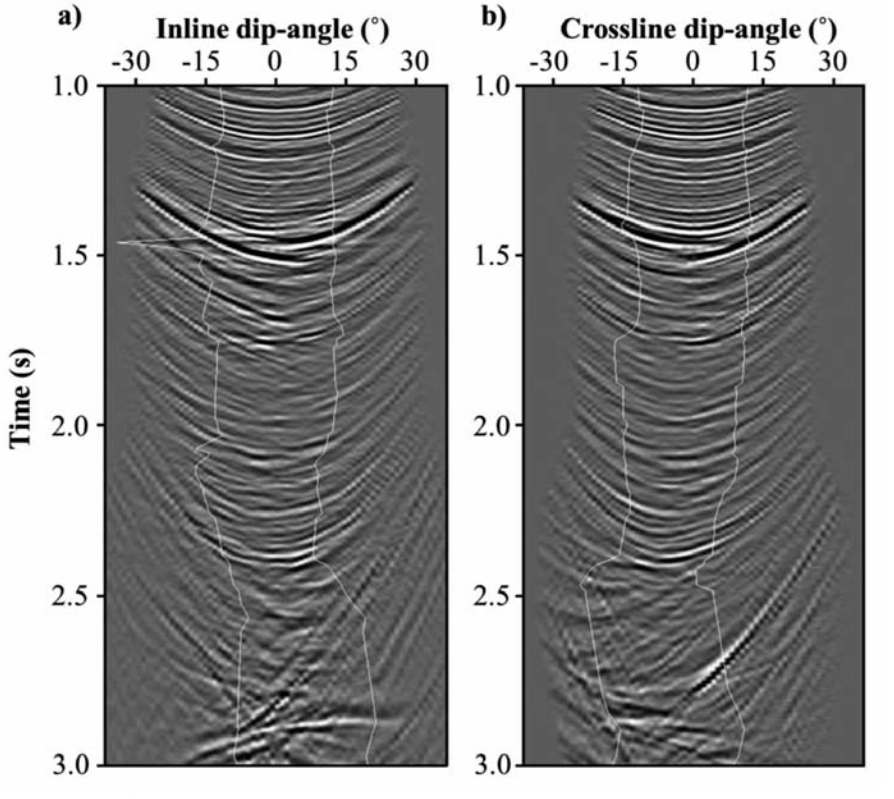

Fig. 7. Dip-angle gathers generated with the proposed method with the Fresnel zone estimated. The two white lines in (a) and (b) denote the upper and lower limits of the Fresnel zones in each direction. The events outside the estimated Fresnel zones will be muted before summation.

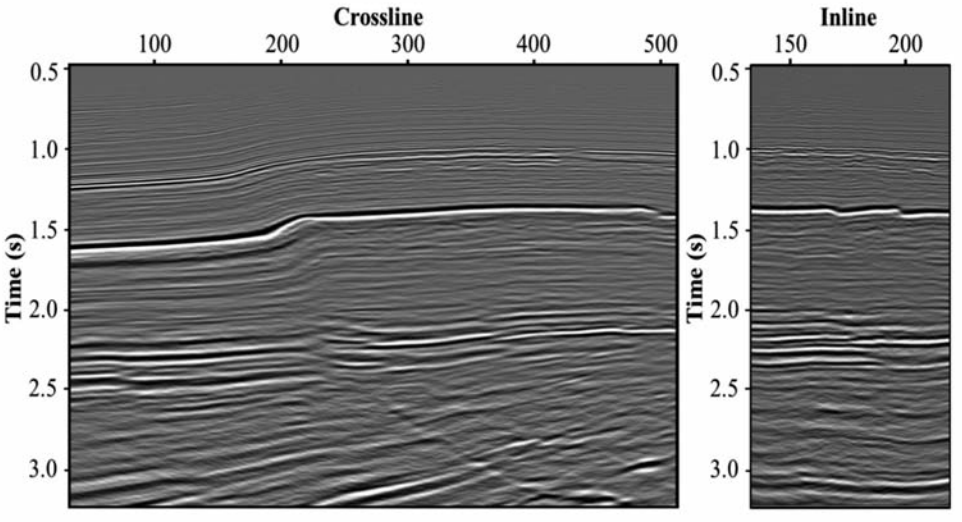

Fig. 8. Imaging result of inline 181 and crossline 341 obtained by stationary-phase 3D VTI PSTM. Note that the main events and faults are well imaged.

CONCLUSION

We present a new VTI PSTM method implemented with stationary theory to improve signal to noise ratio of imaging result, which only stack within the Fresnel zones for the migrated imaging gathers in dip-angle domain. The scheme is developed by incorporating a dip-angle domain stationary-phase implementation into conventional VTI PSTM. We estimate the 2D Fresnel zones used by 3D stationary-phase VTI PSTM through auto-picking technique at each node of a coarser horizontal grid. The 2D Fresnel zones in terms of two dip-angles are obtained. No reflector dips are needed in advance for determining the 2D Fresnel zones. A simple and efficient automated technique of identifying flat events has been presented to pick up the Fresnel zones, which ensures the practicability of stationary-phase VTI PSTM.

We apply the stationary-phase VTI PSTM to a real 3D dataset. Compared with the result from conventional VTI PSTM, the result of stationary-phase VTI PSTM shows better signal to noise ratio.

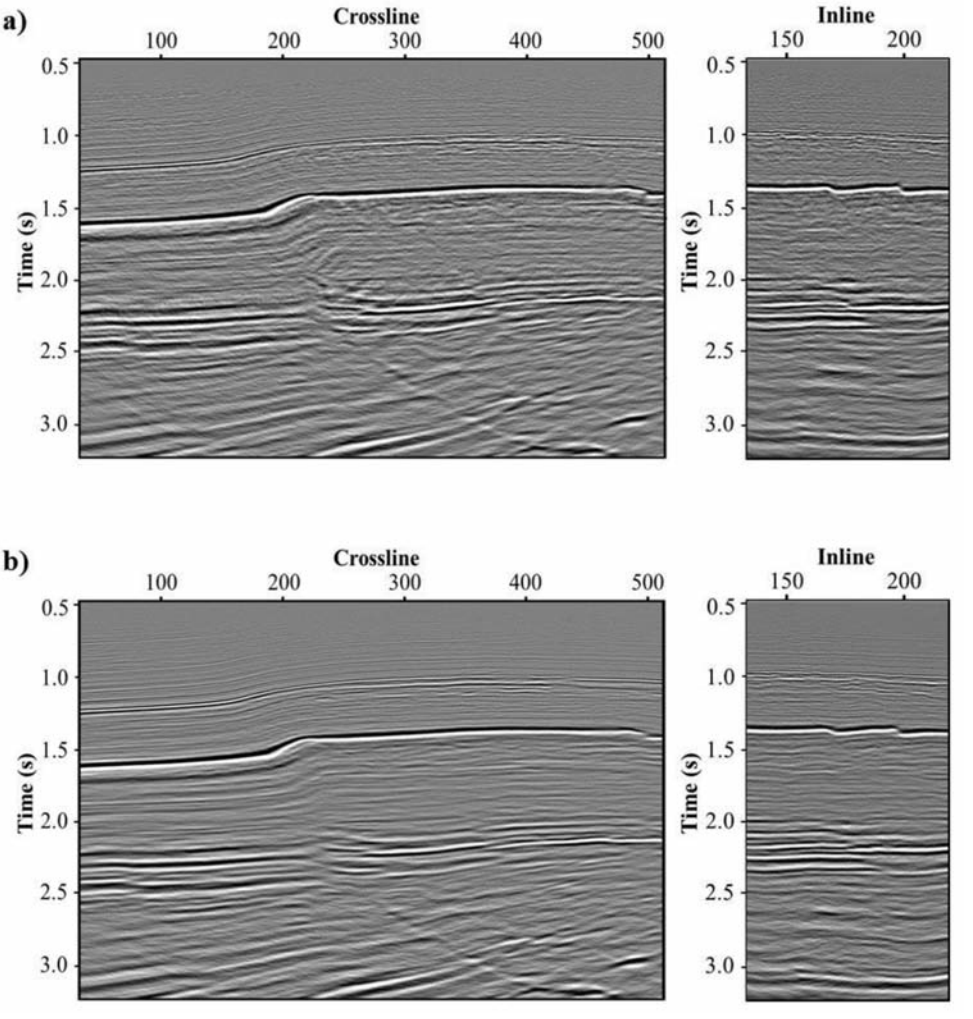

Fig. 9. Imaging result comparison of inline 181 and crossline 341: (a) conventional 3D VTI PSTM; (b) 3D VTI PSTM with optimal summation. Note that the main events and faults are maintained while the noise level has been reduced.

ACKNOWLEDGEMENTS

The authors are grateful to the National Natural Science Fund of China (under grant 41604120), the National Major Project of China (under grant 2017ZX05008-007) and the China Postdoctoral Science Foundation (under grant 2017M610982) for supporting this work. The authors thank the China National Petroleum Corporation for providing the 3D land dataset.

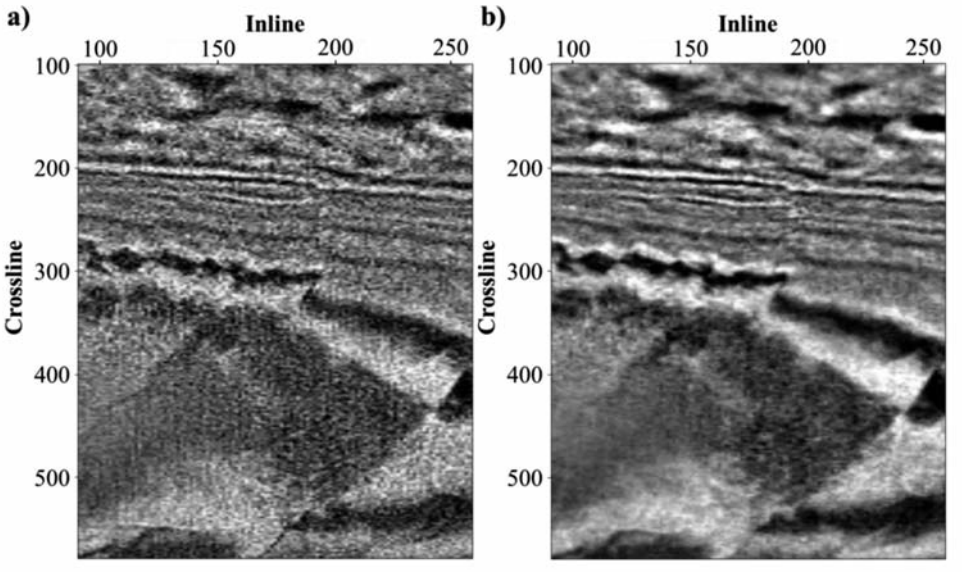

Fig. 10. Comparison of time slice at 2.3 s between (a) conventional VTI PSTM result and (b) VTI PSTM with optimal summation. From the time-slice we note that the faults are more visible to interpret and events become easier to trace.

REFERENCES

Alkhalifah, T. and Tsvankin, I., 1995. Velocity analysis for transversely isotropic media. Geophysics, 60: 1550-1566.

Bleistein, N., 1984. Mathematical Methods for Wave Phenomena. Academic Press, Inc., New York.

Buske, S., Gutjahr, S. and Sick, C., 2009. Fresnel volume migration of single-component seismic data. Geophysics, 74(6): WCA47.

Chen, J., 2004. Specular ray parameter extraction and stationary-phase migration. Geophysics, 69: 249-256.

Claerbout, J.F., 1985. Imaging the Earth's Interior. Blackwell Scientific Publications, New York.

Deng, F. and McMechan, G.A., 2007. True-amplitude prestack depth migration. Geophysics, 72: S155-S166.

Docherty, P., 1991. A brief comparison of some Kirchhoff integral formulas for migration and inversion. Geophysics, 56: 1164-1169.

Gazdag, J., 1978. Wave-equation migration with the phase shift method. Geophysics, 43: 1342-1351.

Giboli, M., Baina, R. and Landa, E., 2013. Depth migration in the offset-aperture domain: optimal summation. Expanded Abstr., 83rd Ann. Internat. SEG Mtg., Houston: 3866-3871.

Klokov, A. and Fomel, S., 2012a. Optimal migration aperture for conflicting dips. Expanded Abstr., 82nd Ann. Internat. SEG Mtg., Las Vegas: 2012-0504.

Klokov, A. and Fomel, S., 2012b. Separation and imaging of seismic diffractions using migrated dip-angle gathers. Geophysics, 77: S131-S143.

Landa, E., Fomel, S. and Reshef, M., 2008. Separation, imaging, and velocity analysis of seismic diffractions using migrated dip-angle gathers. Expanded Abstr., 78th Ann. Internat. SEG Mtg., Las Vegas: 2176-2180.

Marfurt, K.J., 2006. Robust estimates of 3D reflector dip and azimuth. Geophysics, 71: P29-P40.

Okoye, P.N. and Uren, N.F., 1992. Spatial resolution in anisotropic media. Explor. Geophys., 23: 255-260.

Schleicher, J., Hubral, P., Tygel, M. and Jaya, M.S., 1997. Minimum apertures and Fresnel zones in migration and demigration. Geophysics, 62: 183-194.

Sun, H. and Schuster, G.T., 2001. 2-D wavepath migration. Geophysics, 66: 1528-1537.

Sun, J., 1998. On the limited aperture migration in two dimensions. Geophysics, 63: 984-994.

Sun, J. 1999. On the aperture effect in 3D Kirchhoff-type migration. Geophys. Prosp., 47: 1045-1076.

Tillmanns, M. and Gebrande, H., 1999. Focusing in prestack isochrone migration using instantaneous slowness information. Pure Appl. Geophys., 156: 187-206.

Tsvankin, I., 1996. P-wave signature and notation for transversely isotropic media: an overview. Geophysics, 61: 467-483.

Yu, Z., Etgen, J., Whitcombe, D., Hodgson, L. and Liu, H., 2013. Dip-adaptive operator anti-aliasing for Kirchhoff migration. Expanded Abstr., 83rd Ann. Internat. SEG Mtg., Houston: 3692-3695.

Zhang, J. and Zhang, J., 2012. Amplitude-preserved pre-stack time migration in 3D VTI media. Explor. Geophys., 43: 171-177.

Zhang, J.F., Li, Z.W., Liu, L.N., Wang, J. and Xu, J.C., 2016. High-resolution imaging: An approach by incorporating stationary-phase implementation into deabsorption prestack time migration. Geophysics, 81(5): S317-S331.

APPENDIX A

THEORY OF AMPLITUDE-PRESERVED 3D VTI PSTM

In VTI media, Alkhalifah and Tsvankin (1995) suggested that the exact P-wave $V_{nmo}(P)$ depends only on $V_{nmo}(0) = V_{P0}\sqrt{(1+2\delta)}$ and a new effective coefficient $\eta = (\varepsilon-\delta)/(1+2\delta)$. The formula for the P-wave phase velocity derived by Tsvankin (1996) is described as:

$$V^2(\theta)/V_{P0}^2 = 1 + \varepsilon\sin^2\theta - (f/2)$$

$$+ (f/2)\sqrt{\{[1+2\varepsilon\sin^2\theta/f]^2 - [2(\varepsilon-\delta)\sin^2 2\theta/f]\}} \quad , \qquad \text{(A-1)}$$

where $V(\theta)$ is the phase velocity, θ is the phase angle, $f = 1 - V_{S0}^2/V_{P0}^2$.

Based on phase-shift theory (Gazdag, 1978; Claerbout, 1985), the extrapolation of the source or the receiver wavefield in the F-K domain is given by:

$$\tilde{P}(p_x,p_y,\omega,T = \sum_{i=1}^{n}\Delta T_i)$$

$$= f(\omega)\exp[-j\omega\sum_{i=1}^{n}\Delta T_i\sqrt{\{1-v_i^2(p_x^2+p_y^2)/[1-2\eta_i v_i^2(p_x^2+p_y^2)]\}}] \quad , \qquad \text{(A-2)}$$

$$\sum_{i=1}^{n}[\Delta T_i\sqrt{\{1 - v_{nmo}^2(i)(p_x^2+p_y^2)/[1-2\eta_i v_{nmo}^2(i)(p_x^2+p_y^2)]\}}]$$

$$\approx \sqrt{\{1 - V_{nmo}^2(p_x^2+p_y^2)/[1-2\eta_{eff}V_{nmo}^2(p_x^2+p_y^2)]\}}\cdot[\sum_{i=1}^{n}\Delta T_i] \quad . \qquad \text{(A-3)}$$

Substituting eq. (A-3) into (A-2) and then applying the spatial inverse Fourier transform that yield

$$P(x,y,\omega,T) = (\omega/4\pi^2)\int\int f(\omega)\exp$$

$$\{-j\omega[\sqrt{\{1-V_{nmo}^2(p_x^2+p_y^2)/[1-2\eta_{eff}V_{nmo}^2(p_x^2+p_y^2)]\}}\cdot T - p_x x - p_y y]\}dp_x dp_y \quad , \qquad \text{(A-4)}$$

where p_x and p_y denote the ray parameters in the x- and y-directions in the Cartesian coordinates, respectively. According to the stationary-phase theory (Bleistein, 1984; Doherty, 1991) and we seek the stationary-phase solution of

the integral that yields

$$p_0 = (x^2 + y^2)/V_{nmo}^2 T^2 \ , \quad p_1 = p_0/(p_0 + 1) \ ,$$

$$\xi = \sqrt{\{[p_0^3 + 6p_0^2 + 9p_0 + 4 - \eta_{eff}(6p_0^2 - 12p_0)]/} \qquad \text{(A-5)}$$

$$[p_0^3 + 6p_0^2 + 9p_0 + 4 + \eta_{eff}(2p_0^3 + 10p_0^2 + 44p_0)]\} \ .$$

Then the traveltime and amplitude can be expressed as

$$\tau = [\sqrt{\{1 - \xi^2 p_1/(1 - 2\eta_{eff}\xi^2 p_1)\}} + \xi\sqrt{(p_0 p_1)}]^T \ , \qquad \text{(A-6)}$$

and

$$A = \{(1 - 2\eta_{eff}\xi^2 p_1)^2[1 - (2\eta_{eff}+1)\xi^2 p_1]\}/$$

$$TV_{nmo}^2\sqrt{\{1 + 4\eta_{eff}\xi^2 p_1 - 6\eta_{eff}(2\eta_{eff} + 1)\xi^4 p_1^2\}} \ . \qquad \text{(A-7)}$$

Although the theory is developed for layered-media, eqs. (A-6) and (A-7) can be used for inhomogeneous anisotropic media with lateral variations of V_{nmo} and η_{eff}.

Since we have derived the traveltime and amplitude coefficient then we have the imaging result as

$$I(x,y,T) = (A_r/A_s) \int f(\omega)\omega\exp[-j(\pi/2)]\exp[-j\omega(t_s+t_r)]d\omega$$

$$= (A_r/A_s)F'(t_s+t_r) \ , \qquad \text{(A-8)}$$

where $F'(t)$ is the first-order time derivative of time series of a trace, i.e., the first-order time derivative of the inverse Fourier transform of $f(\omega)$, A_s and t_s are amplitude and traveltime of wavefield from source position $(x_s,y_s,0)$ to imaging position (x, y, T), A_r and t_r are amplitude and traveltime of wavefield from receiver position to imaging position.

APPENDIX B

FRESNEL ZONES IN 2D DIP-ANGLE GATHERS

Fig. 1 gives the illustration of dip-angle gather generation. Let θ_x and θ_y be the inline and crossline dip-angles of the reflector (i.e., the apparent dips of the reflector in the x-z and y-z planes), respectively. We have the direction cosines of the vector from point P to Q on reflector Π as

$$l = \cos\alpha/\sqrt{\{1 + (\tan\theta_x\cos\alpha+\tan\theta_y\sin\alpha)^2\}} \quad , \tag{B-1a}$$

$$m = \sin\alpha/\sqrt{\{1 + (\tan\theta_x\cos\alpha+\tan\theta_y\sin\alpha)^2\}} \quad , \tag{B-1b}$$

$$n = (\tan\theta_x\cos\alpha + \tan\theta_y\sin\alpha)/\sqrt{\{1 + (\tan\theta_x\cos\alpha+\tan\theta_y\sin\alpha)^2\}} \quad , \tag{B-1c}$$

where α denotes the azimuth angle of plane QOP. Let the length of vector $\overline{PQ}$ be d. The coordinates of point Q can be expressed as $(x_p+dl, y_p+dm, T_p+dn/v)$. Here, (x_p, y_p, T_p) is the coordinate of imaging point P with T_p denoting the one-way vertical traveltime, and v is the interval velocity at point P.

For simplicity we replace (θ_x, θ_y) with the traveltime related dip-angle in eq. (B-1) and let $\rho \approx v/V_{rms}$ then we approximately obtain the coordinates of point Q as

$$x_Q \approx x_p + d\cos\alpha/\sqrt{\{1 + (\tan\varphi_x\cos\alpha + \tan\varphi_y\sin\alpha)^2\}} \quad , \tag{B-2a}$$

$$y_Q \approx y_p + d\sin\alpha/\sqrt{\{1 + (\tan\varphi_x\cos\alpha + \tan\varphi_y\sin\alpha)^2\}} \quad , \tag{B-2b}$$

$$T_Q \approx T_p + d(\tan\varphi_x\cos\alpha + \tan\varphi_y\sin\alpha) \\ /V_{rms}\sqrt{\{1 + (\tan\varphi_x\cos\alpha + \tan\varphi_y\sin\alpha)^2\}} \quad . \tag{B-2c}$$

Due to the fact that curve SQ denotes the coincided scattered and incident rays, traveltime equality from point S to Q and O gives

$$\{[(x_Q - x_S)^2 + (y_Q - y_S)^2]/V_{rms}^2\} + T_Q^2 \\ = \{[(x_P - x_S)^2 + (y_P - y_S)^2]/V_{rms}^2\} + (T_p - t)^2 \quad , \tag{B-3}$$

where t denotes the time difference for determining the limits of the Fresnel zone, which is governed by the maximum or dominant frequency of the migrated event.

Substituting eqs. (B-2) into (B-3) yields

$$x_S \approx x_P + d\{[\cos\alpha(1+\tan^2\gamma_x) + \tan\gamma_x \tan\gamma_y \sin\alpha]$$

$$/\sqrt{[1 + (\tan\gamma_x\cos\alpha + \tan\gamma_y\sin\alpha)^2]}\} + V_{rms}T_p\tan\gamma_x \quad , \qquad \text{(B-4a)}$$

$$y_S \approx y_P + d\{[\sin\alpha(1+\tan^2\gamma_y) + \tan\gamma_x \tan\gamma_y \cos\alpha]$$

$$/\sqrt{[1 + (\tan\gamma_x\cos\alpha + \tan\gamma_y\sin\alpha)^2]}\} + V_{rms}T_p\tan\gamma_y \quad , \qquad \text{(B-4b)}$$

where

$$d = V_{rms}\sqrt{(2tT_p - t^2)} \quad . \qquad \text{(B-5)}$$

We obtain the limits of the Fresnel zone in terms of traveltime related dip-angle φ_x and φ_y by substituting the coordinates of point S and O into eq. (5) as

$$\tan\varphi_x = [T_p\tan\gamma_x/(T_p - t)] + \sqrt{(2tT_p - t^2)}/(T_p - t)$$

$$\times [\cos\alpha(1+\tan^2\gamma_x) + \tan\gamma_x \tan\gamma_y \sin\alpha]$$

$$/\sqrt{[1 + (\tan\gamma_x\cos\alpha + \tan\gamma_y\sin\alpha)^2]} \quad , \qquad \text{(B-6a)}$$

$$\tan\varphi_y = [T_p\tan\gamma_y/(T_p - t)] + \sqrt{(2tT_p - t^2)}/(T_p - t)$$

$$\times [\sin\alpha(1+\tan^2\gamma_y) + \tan\gamma_x \tan\gamma_y \cos\alpha]$$

$$/\sqrt{[1 + (\tan\gamma_x\cos\alpha + \tan\gamma_y\sin\alpha)^2]} \quad . \qquad \text{(B-6b)}$$

Eqs. (B-6) gives the limits of the Fresnel zone at point P in terms of two traveltime related dip-angles at different azimuth angles.